AIAA JOURNAL
Vol. 46, No. 6, June 2008

Technical Notes

TECHNICAL NOTES are short manuscripts describing new developments or important results of a preliminary nature. These Notes should not exceed 2500 words (where a figure or table counts as 200 words). Following informal review by the Editors, they may be published within a few months of the date of receipt. Style requirements are the same as for regular contributions (see inside back cover).

Delta-Wing Flow Control Using Dielectric Barrier Discharge Actuators

David Greenblatt*
Technion—Israel Institute of Technology, 32000 Haifa, Israel
and
Y. Kastantin,† C. N. Nayeri,‡ and C. O. Paschereit§
Technical University of Berlin, 10623 Berlin, Germany

DOI: 10.2514/1.33808

Nomenclature

C_D	=	drag force coefficient
C_L	=	lift force coefficient
C_N	=	surface normal force coefficient
C_T	=	surface tangential force coefficient
C_μ	=	momentum coefficient, time-mean component, J/cq_∞
$\langle C_\mu \rangle$	=	momentum coefficient, oscillatory component, $\langle J \rangle / cq_\infty$
c	=	model chord length
DC	=	duty cycle
F^+	=	reduced excitation frequency, $f_m c/U_\infty$
f	=	plasma driving frequency
f_m	=	pulsed-modulation frequency
J	=	time-mean component of jet momentum
$\langle J \rangle$	=	oscillatory component of jet momentum
q_∞	=	freestream dynamic pressure
Re	=	Reynolds number based on chord length
s	=	model semispan length
s_L	=	local semispan length at corresponding x/c
t	=	wing thickness
U,V,W	=	chordwise coordinate system
U_p	=	plasma-jet velocity
U_∞	=	freestream velocity
x, y, z	=	chordwise coordinate system
x', y', z	=	leading-edgewise coordinate system
α	=	angle of attack
Λ	=	delta-wing sweepback angle
ϕ	=	control-cycle phase angle
ω_x	=	streamwise vorticity, $\partial W/\partial y - \partial V/\partial z$

Presented as Paper 4277 at the 25th AIAA Applied Aerodynamics Conference, Miami, FL, 25–28 June 2007; received 1 August 2007; revision received 21 December 2007; accepted for publication 23 December 2007.

*Senior Lecturer, Faculty of Mechanical Engineering, Technion City; davidg@technion.ac.il. Senior Member AIAA.
†Graduate Student, 8 Mueller Breslau Street.
‡Research Assistant, 8 Mueller Breslau Street. Senior Member AIAA.
§Professor, Chair of Experimental Fluid Dynamics, 8 Mueller Breslau Street. Senior Member AIAA.

I. Introduction

FLOW over the sharp leading edges of a delta wing at high angles of attack separates and forms shear layers that roll up into two large vortices, which are primarily responsible for lift generation at low speeds. These vortices are only weakly dependent on Reynolds number when the leading edge is sharp [1]. As the angle of attack increases, the swirl velocity of the vortices also increases. When the ratio of swirling velocity to axial velocity at any point in the vortex exceeds approximately 1.3, the vortex breaks down; that is, it expands into a highly fluctuating structure in which the velocity components are drastically reduced in the central part of the structure [1]. Consequently, vortex breakdown is generally associated with delta-wing stall and can induce vibrations resulting in tail buffet, loss of control, and possible wing damage.

A number of investigators have suggested that shear-layer instabilities are linked with both the development of leading-edge vortices and their breakdown [2,3]. Vortices that have undergone breakdown can be viewed as curved shear layers, and perturbations introduced along the leading edge profoundly affect them, producing significant changes to the wing's normal force [4]. The underlying mechanism of performance enhancement by periodic excitation on a delta wing is unclear, with speculations ranging from delay of vortex breakdown to vortex enhancement. It was suggested in [5] that vortex breakdown could be delayed by about 25% of the chord by introducing periodic perturbations at the leading edge. In contrast, water-tunnel particle image velocimetry (PIV) data [6] suggest that the vortex-breakdown location is not altered, but that the downstream directed velocity close to the surface is increased, thereby decreasing the upper-surface pressure. A follow-up study [7] ascertained that excitation from the aft half of the leading edge in the vicinity of the vortex-breakdown location was most effective. PIV measurements revealed that the shear layer transports high streamwise momentum fluid into the wake, downstream of the breakdown location. The most detailed study appears to be that of [4], in which cavity-installed piezoelectric actuators were employed to effect control. Optimum performance was achieved when the high resonance frequency was burst-modulated to produce $F^+ \sim \mathcal{O}(1)$, with duty cycles (DCs) around 5%. Two-dimensional PIV measurements suggested that excitation enhances the momentum transfer across the shear layer, downstream of the original vortex-breakdown location, generating a streamwise vortex for which the size is commensurate with the local wingspan.

For delta wings or swept planforms with a low aspect ratio and at low Reynolds numbers [typical of some micro air vehicles (MAVs)], leading-edge vortices also serve as a dominant mechanism of lift generation. It therefore stands to reason that periodic excitation may be effective for enhancing MAV performance or controlling flight. However, on vehicles of this size (typically, ≤ 15 cm), it may be impractical to install zero-mass-flux actuators within the vehicle structure or to attach oscillators to the surface. In these instances, dielectric barrier discharge (DBD) actuators [8,9] emerge as a strong candidate for leading-edge vortex control. Previous work by some of the authors of this Note [10–12] demonstrated the effectiveness of such actuators on airfoils at $Re < 100,000$ (or $U_\infty < 10$ m/s), consistent with typical MAV Reynolds numbers.

The present limited investigation addressed two specific objectives. The primary objective was to maximize delta-wing performance at low speeds ($Re \leq 75,000$) using leading-edge DBD

plasma actuation. The secondary objective involved an investigation of the flowfield corresponding to conditions under which active control was most effective, within the limitations of the actuation methods employed here. To achieve this, a semispan delta-wing model was constructed, equipped with a leading-edge DBD actuator, and wind-tunnel-tested. The flowfield was interrogated by means of flow visualization, PIV, and laser Doppler anemometry (LDA). The present Note differs from the original conference paper [13] in the following respects: the preliminary Gurney flap data are not included, the conventional DBD actuator was eliminated, and the actuator calibration was repeated based on a more accurate measurement and data processing technique. These items are subsequently discussed further.

II. Experimental Setup

Measurements were conducted in the test section of a 400×280 mm blowdown-type wind tunnel, driven by a 1-kW radial blower, with a 0.8–10-m/s velocity range. The tunnel incorporated a 6.25:1 contraction ratio, and the turbulence level did not exceed 0.15%. A three-component aluminum bending-beam strain-gauge-type balance was mounted on top of the test section, and the delta-wing model was attached vertically to the balance by means of the sting. The model was constructed from 2-mm-thick fiberglass with a 200-mm chord, a 60-deg sweep angle, and a sharp leading edge (Fig. 1a). A DBD plasma actuator was deployed at the leading edge (see Fig. 1b). The configuration of the actuator differed somewhat from those commonly employed in published studies (e.g., [8,9]). In the original study [13], the common configuration was tested, with no significant effect on wing performance measured; hence, that configuration was not tested in detail. For all data reported herein, the encapsulated and exposed electrodes (both 70 μm thick) were mounted on opposite surfaces of the wing, separated by three layers of 50-μm-thick Kapton tape (Fig. 1b), and this arrangement

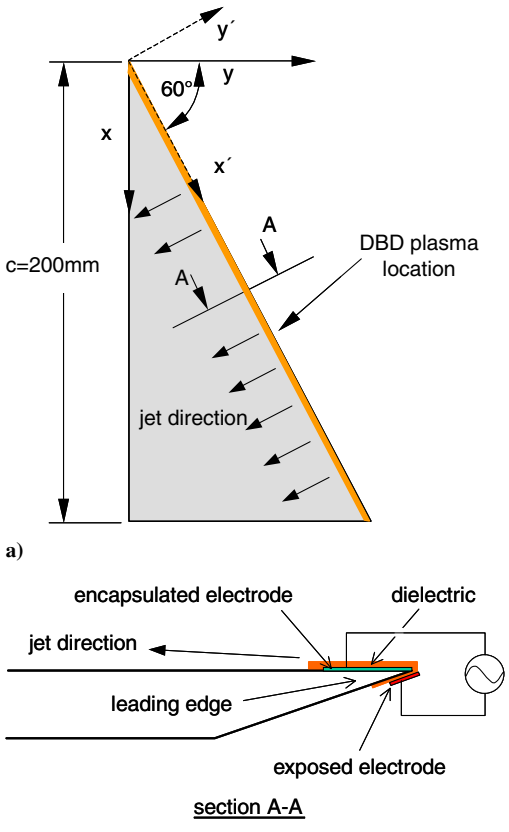

Fig. 1 Schematic of the semispan delta-wing model: a) top-view showing the dimensions and coordinate system and b) layout of the DBD plasma actuator at the wing leading edge.

produced a plasma-induced jet inboard from the leading edge, as indicated in Figs. 1a and 1b. The maximum uncertainty associated with the aerodynamic coefficients was ± 0.015 at the lowest Reynolds number tested: namely, $Re = 20,000$. The actuator output in terms of momentum was calibrated by direct measurement using a two-dimensional LDA, and this is described in Sec. III.

In addition to model load measurements, two-dimensional PIV was performed above the model upper surface at locations $x/c = 0.2, 0.5$, and 0.8. The PIV measurement planes were normal to the surface and root chord line. For the optimum control case, additional phase-averaged data were acquired at $x/c = 0.5$. Measurements were made with two Nd:YAG 17-mJ lasers and a 1024×1024 pixel CCD camera. Data were processed in 32×32 pixel interrogation areas with 50% overlap. A commercial seed-particle generator was used to generate particles with an average diameter of 1 μm. Interrogation areas were cross-correlated, and a local median filter was used to eliminate spurious vectors. The eliminated data were replaced via interpolation from the adjacent interrogation areas. The resulting vector field was used for an adaptive cross-correlation of the data, spurious data were filtered again, and the adaptive cross-correlation was reapplied. The percentage of spurious vectors never exceeded 2% for any measurement plane.

III. Actuator Calibration

The actuator was calibrated (i.e., its momentum output was directly measured) before the wind-tunnel investigation. This was achieved by placing the model in a Plexiglas box ($60 \times 40 \times 20$ cm) and measuring the wall jet produced by the actuator using LDA. The calibration was carried out at five locations along the leading edge in the range of $0.15 \leq x'/c \leq 0.85$ at 3, 5, and 7 mm downstream of, and normal to, the trailing edge [13]. At distances less than approximately 3 mm from the actuator, no data were measurable, because the LDA probe volume was located in the plasma sheath. Moreover, profiles acquired further downstream of the actuator indicated, as expected, that the wall jet loses momentum. Consequently, the calibration was based on the momentum generated at $y' = 3$ mm downstream of the actuator, measured at five locations along the leading edge.

For all data acquired, the actuator was driven in pulsed-modulation mode (i.e., square-wave modulation), because it was shown in [4] that this mode was superior to other wave forms using zero-mass-flux jets. In the conference paper [13], the pulsed-mode calibration was based on the assumption that the actuator responds instantaneously to the drive signal. Direct calibration, however, showed that this introduced unacceptably large errors. Consequently, the momentum coefficients reported here are based on a direct calibration of the actuator for a wide range of pulsation frequencies and duty cycles, and this calibration procedure is described in detail in [12]. It was observed in [12] that the direct analogy of a pulsed DBD actuator with zero-mass-flux blowing is an oversimplification, because the actuator produces both time-mean and oscillatory momentum. In this sense, it is analogous to a nonzero-mass-flux pulsed jet, in which the relative momentum coefficients are denoted as $(C_\mu, \langle C_\mu \rangle)$ [12]. The relative magnitude of these two coefficients can have a profound effect on airfoil and wing performance.

With the exception of the data acquired at $x'/c = 0.15$, the momentum variation along the leading did not exceed a 20% deviation from the mean in the region defined by $0.35 \leq x'/c \leq 0.85$. The relatively small variations in jet momentum were traced to changes in dielectric properties resulting from dielectric heating of the glue used to bond the Kapton tape strips to one another.

IV. Discussion of Results

A. Baseline Performance

Given the low Reynolds number range, the model performance in terms of C_N, C_L, and C_D was reasonably independent of the

Reynolds number [13]. This was attributed to the sharp leading edge, which ensured a fixed separation and roll-up of the leading-edge vortex. Up to $\alpha \approx 24$ deg, the normal force coefficient was comparable with that of [4], but stall occurred at a somewhat lower angle, resulting in a somewhat lower $C_{L,\max}$ [13]. This was attributed to a combination of the low Reynolds number and relatively thin ($t/c = 1\%$) wing employed here.

B. Dependence on Control Parameters

As is common in active flow control studies, the effect of the plasma-induced jet on poststall performance was assessed by performing a frequency scan with the wing at a relatively large poststall angle of attack (i.e., $\alpha = 36$ deg). This angle is representative of *deep stall* (typically, more than 10 deg beyond the static stall angle), in which the vortex is completely broken down (see Sec. IV.C). The results for normal force and lift coefficients for a range of Reynolds numbers are shown in Fig. 2a and 2b. These data are broadly consistent with the zero-mass-flux study of [4], with some differences in the details. First, there is a more clearly defined peak at $F^+ \approx 1$; this is true for $Re \leq 50,000$, presumably because the forcing amplitude is sufficiently large and exceeds a threshold $\langle C_\mu \rangle$. Second, the larger $\langle C_\mu \rangle$ that results from lower Reynolds numbers does not change the basic form of the curves, but generally produces performance enhancement; nevertheless, there is a small, but surprising, drop in performance between $Re = 35,000$ and 20,000. It should be expected that the relative increase in $\langle C_\mu \rangle$ would improve performance. Finally, in the piezo study, changes to the lift coefficient were not reported, and although it was stated that no meaningful $C_{L,\max}$ were observed, poststall C_L increases by 0.2 here.

Further insight into the actuator's operation and into the performance differences between $Re = 35,000$ and 20,000 can be gained by considering the duty-cycle scan shown in Figs. 3a and 3b

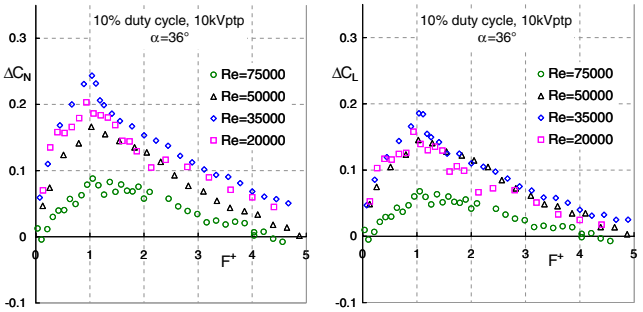

Fig. 2 Dependence of a) normal force coefficient and b) lift coefficient at reduced frequency, for different Reynolds numbers with the wing at a poststall angle of attack.

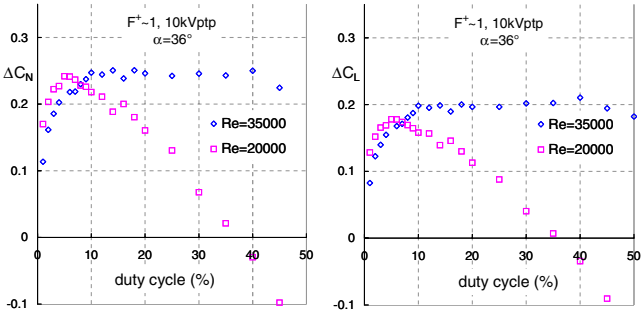

Fig. 3 Dependence of a) normal force coefficient and b) lift coefficient on duty cycle, for different Reynolds numbers, with the wing at a poststall angle of attack.

for $F^+ \approx 1$. The corresponding calibrated momentum coefficients are shown in Table 1 (see [12] for calibration-method details). A sharp rise in C_N and C_L at a low DC is observed at both Reynolds numbers, which is consistent with an equally sharp rise in the momentum produced by the actuator in the range of $0 \leq \text{DC} \leq 5\%$. On airfoils, it is commonly observed that a threshold $\langle C_\mu \rangle \sim 0.1\%$ should be exceeded for effective flow control [14], and this is also observed here. As the DC increases, $\langle C_\mu \rangle$ crosses a threshold above which it becomes dominant and excites the unsteady-lift mechanism (see Sec. IV.C). With zero-mass-flux jets, once the threshold is exceeded, leading-edge control effectively saturates and an increase in momentum by 1 order of magnitude has a relatively small effect [14]. In the present context, the actuators produce both steady and oscillatory components of momentum and hence as the DC increases the effect is dramatically different, depending upon the Reynolds number (see the steady and unsteady momentum coefficients in Table 1).

At $Re = 20,000$ for DC > 5%, the continuous increase in the steady momentum coefficient begins to dominate and gradually reduces and ultimately destroys the unsteady-lift enhancement mechanism; for DC ≥ 40%, the lift is in fact reduced. At $Re = 35,000$, the steady component does not dominate, due to its reduced value, and hence the unsteady mechanism at $\langle C_\mu \rangle \geq 0.1\%$ is not materially affected. The effect of the magnitude of the mean and oscillatory-momentum coefficients is illustrated by observing that both coefficients are similar for DC = 10 and 40% at the lower and higher Reynolds numbers, respectively (see Table 1); consequently, similar normal force and lift coefficients result (see Figs. 3a and 3b). At $Re = 75,000$, the oscillatory-momentum coefficient is relatively small $\langle C_\mu \rangle = 0.04\%$ and, consequently, has only a small effect on wing performance, as shown in Figs. 2a and 2b.

Wing performance as a function of α is shown for $Re = 20,000$ and 35,000 in Figs. 4a–4c, in which control is applied at close to the optimum conditions $F^+ \approx 1$ and DC = 10%. As expected, the normal force coefficient shows a substantial increase in its maximum value of approximately 0.2. Unlike previous investigations, there is also an increase in $C_{L,\max}$ of approximately 0.1 and a reduction in C_D. These data clearly have implications for delta-wing poststall control and maneuverability, as well as for minimum takeoff and landing speeds. It is unlikely that the drag reduction observed here results from the momentum of the actuator, because at DC = 10%, the maximum combined momentum output in the stream direction is $(C_\mu + \langle C_\mu \rangle) \cos \Lambda \sim 0.004$ and ~0.001 at $Re = 20,000$ and 35,000, respectively (see Table 1).

C. Flowfield Measurements and Data Analysis

An attempt to gain understanding of the control mechanism was undertaken by performing two-dimensional PIV measurements in the y–z plane at $x/c = 0.2$, 0.5, and 0.8 (Figs. 5–7, respectively). Detailed phase-averaged data were acquired at $x/c = 0.5$ for 45-deg intervals of the control cycle (Figs. 8a–8h). All PIV data are shown from behind the wing, looking upstream, and the coordinates of each data set are measured from the leading edge and nondimensionalized with respect to the local wingspan s_L. For the present case, the wing is

Table 1 Steady and oscillatory-momentum coefficients (percentages) as a function of duty cycle for selected Reynolds numbers at $F^+ \approx 1$

	$Re = 20,000$		$Re = 35,000$		$Re = 75,000$	
Duty cycle, %	C_μ	$\langle C_\mu \rangle$	C_μ	$\langle C_\mu \rangle$	C_μ	$\langle C_\mu \rangle$
1	<0.01	<0.01	<0.01	<0.01	<0.01	<0.01
3	0.19	0.11	0.06	0.03	~0.01	~0.01
5	0.39	0.34	0.13	0.11	0.03	0.02
10	0.52	0.59	0.17	0.19	0.04	0.04
20	0.95	1.24	0.31	0.40	0.07	0.09
30	1.23	1.52	0.40	0.49	0.09	0.11
40	1.65	1.90	0.53	0.61	0.12	0.13
50	2.08	1.89	0.67	0.61	0.15	0.13

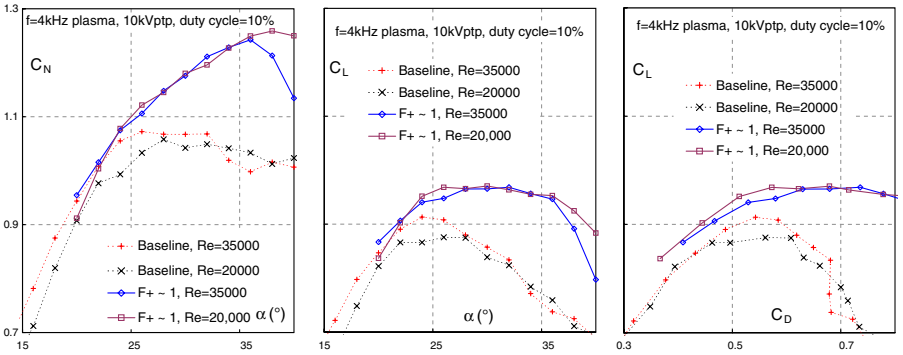

a) b) c)

Fig. 4 Effect of DBD plasma actuation on delta-wing performance, primarily in the poststall regime.

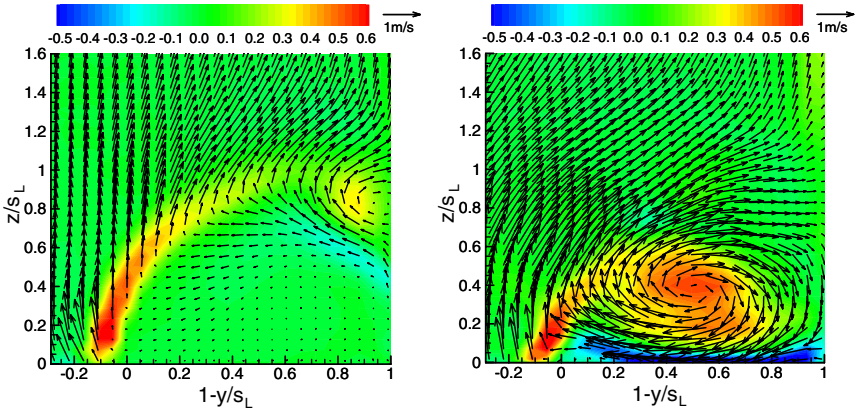

a) b)

Fig. 5 Random-phase PIV vorticity ($\omega_x \times 1000$) and velocity vectors at $\alpha = 36$ deg, $x/c = 0.2$, and $Re = 20,000$ showing baseline (left) and controlled (right) ($F^+ = 1$ and DC = 10%) flowfields in the y–z plane.

well beyond its stall angle, and the separated flow forms a shear layer at the leading edge. In this deep stall state, no remnant of the leading-edge vortex remains (see Figs. 5a, 6a, and 7a). As expected (i.e., consistent with the measured increases to C_N and C_L), control produces a strong effect on the vortex. At the leading edge, the shear layer is oriented inboard and a strong vortex centered at $y/s_L \sim 0.5$ is generated above on the wing surface. The combination of the no-slip conditions near the wall and the velocity field just above the surface, flowing outward toward the leading edge, generates a region of relatively large countersigned vorticity.

A qualitatively similar situation is apparent further downstream ($x/c = 0.5$), in which control is shown for both 5 and 10% duty cycles; the difference between the two control cases is very small, and this is fully consistent with the load measurements shown in Fig. 3a. Nevertheless, there are two important differences between the controlled flowfields at $x/c = 0.2$ and 0.5. First, the shear layer that forms at the leading edge in the later case is not deflected inboard as in the former case. Second, the vortices in the latter case are much more diffuse and significantly weaker; that is, peak vorticity is approximately half of that at $x/c = 0.2$ (note the

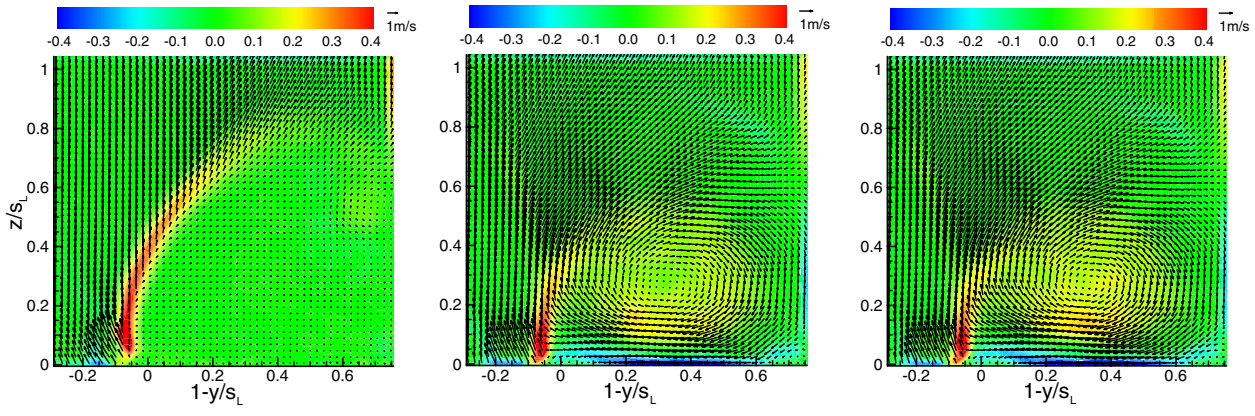

a) b) c)

Fig. 6 Random-phase PIV vorticity ($\omega_x \times 1000$) and velocity vectors at $\alpha = 36$ deg, $x/c = 0.5$, and $Re = 20,000$ showing baseline (left) and controlled (middle: $F^+ = 1$ and DC = 5% and right: $F^+ = 1$ and DC = 10%) flowfields in the y–z plane.

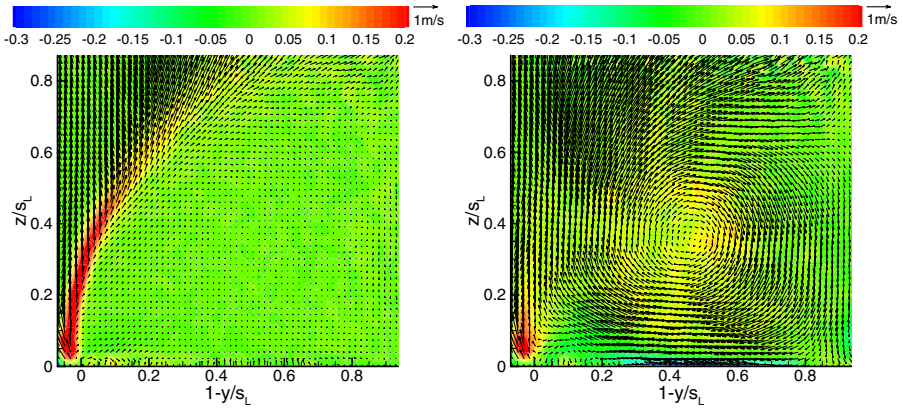

Fig. 7 Random-phase PIV vorticity ($\omega_x \times 1000$) and velocity vectors at $\alpha = 36\,\text{deg}$, $x/c = 0.8$, and $Re = 20,000$ showing baseline (left) and controlled (right) ($F^+ = 1$ and DC = 10%) flowfields in the y–z plane.

different scaling that is used to render the vorticity levels visible). In addition, the vortex is further from the surface: $z/s_L \approx 0.4$ vs 0.3 for $x/c = 0.2$ and 0.5, respectively. This is not immediately clear from the figure, because the coordinates are nondimensionalized with respect to the local span s_L; hence, the relative distance increase from the surface between the two locations is approximately $(0.3/0.4) \times (0.5/0.2) \approx 2$. With increased downstream distance ($x/c = 0.8$), this trend continues with a further reduction in peak vorticity, roughly one-sixth of that at $x/c = 0.2$, and with a greater relative distance from the surface (approximately 3.5). Thus, it can be concluded that the vast majority of vortex lift occurs near the wing apex, perhaps within the first 30% of chord.

The phase-averaged data shown in Figs. 8a–8h furnish some added insight into the mechanism of control. In pulsed mode for DC = 10%, control commences at $\phi = 0\,\text{deg}$ and terminates at $\phi = 36\,\text{deg}$. At $\phi = 0\,\text{deg}$ (Fig. 8a), relatively strong shear is seen at the leading edge and a curved shear layer is evident above the wing surface. This flow state essentially represents the end of the flow control cycle, because this is when the plasma-induced body force is initiated. The resulting effect of this body force, which terminates at $\phi = 36\,\text{deg}$ for the 10% duty cycle, can be seen at $\phi = 45\,\text{deg}$ as the shear layer at the leading edge is significantly deflected inboard, severing it from the remainder of the curved shear layer. Simultaneously, the vortex center moves slightly upward, away from the surface. At $\phi = 90\,\text{deg}$, the shear layer snaps back and reestablishes the curved shear layer. During the remainder of the cycle, the curved shear layer is visible and the vortex traverses an almost circular path with a local diameter of $y/s_L \approx z/s_L \approx 0.2$.

Some understanding of the optimum reduced frequency reported here and the distribution of lift generation along the wing can be gained following the analysis of [15], in which it was assumed that perturbations generated at the leading edge are amplified and convected downstream, normal to the leading edge, much like their two-dimensional counterparts. The effect of sweep enters only through the component of freestream velocity tangential to the wing leading edge. The analysis showed that the perturbation trajectories are swept across the span as a result of the tangential velocity component; hence, perturbations introduced near the apex will have a far greater effect that those introduced at the tip, because the latter will be swept off the wing without producing any meaningful change to the aerodynamic loads. This is fully consistent with the present observations in which the greater load changes were observed near the apex (discussed previously).

The analysis further indicates that just as there is a optimum frequency associated with control using DBD actuators on an unswept wing, there will also be an optimum frequency when sweep is introduced; this is indeed what was observed here. A central difficulty lies in choosing an appropriate length scale in the definition of F^+, because when the conditions normal to the leading edge are used [15,16], the length scale varies from zero at the leading edge to a maximum ($c \cos \Lambda$ is used here), resulting in $F^+ = f_m c/U_\infty$, and then back to zero at the tip. Separation control on an unswept flat plate using a similar DBD actuator indicated an approximate optimum reduced-frequency range: $0.3 \leq F^+ \leq 0.6$ [10–12]. For $F^+ > 1$ on the unswept plate, vortices rolled up near the leading edge and dissipated over a short downstream distance, thus proving ineffective for separation control. It is assumed that a similar mechanism is operating on the delta wing tested here, and this is consistent with the analysis already described. Nevertheless, the observation that the optimum delta wing F^+ is approximately twice that associated with unswept plate indicates that the length scale chosen here (namely, $c \cos \Lambda$) is too large and should be more in keeping with the reattachment location, as suggested by [14].

V. Conclusions

The present study considered the active control of a leading-edge vortex on a semispan delta wing at typical MAV Reynolds numbers by means of a DBD plasma actuator. It is asserted here that studies of this nature can have implications for both MAVs and large-scale aircraft. In the first instance, it is clear that plasma actuation can be employed directly to enhance the performance of MAVs. Generally speaking, laboratory studies employ conventional high-voltage generators in which a key objective is to minimize the power supplied to the actuators. This is mainly due to the difficulty encountered when attempting to develop lightweight systems that can be carried onboard a MAV. Nevertheless, if the power requirements are low enough, lightweight systems can be developed, because high-kilovolt-level voltages are routinely generated in many low-power electronics applications.

In the second instance, due to their surface-application flexibility, DBD actuators can be placed in various orientations and locations with relative ease. There are no other known actuators that have such flexibility. Therefore, studies such as these can have direct relevance to large-scale low-aspect-ratio wings, such as delta-wing aircraft, and can be used for risk-reduction studies. For example, low-cost small-scale wind-tunnel testing can be performed to isolate the optimum control locations, configurations, frequencies, etc., before more expensive large-scale or full-scale testing. The main premise is that at low speeds (for example, for landing and high-alpha maneuvers such as low-Mach-number, mildly compressible, flows), the flow separates from the leading edge of a delta wing at high Reynolds numbers, much like it does at low Reynolds numbers. Thus, actuator placement, relative momentum addition (C_μ and $\langle C_\mu \rangle$), etc., can be considered to be relevant at the large scale, to a first approximation, at flight Reynolds numbers under mildly compressible conditions.

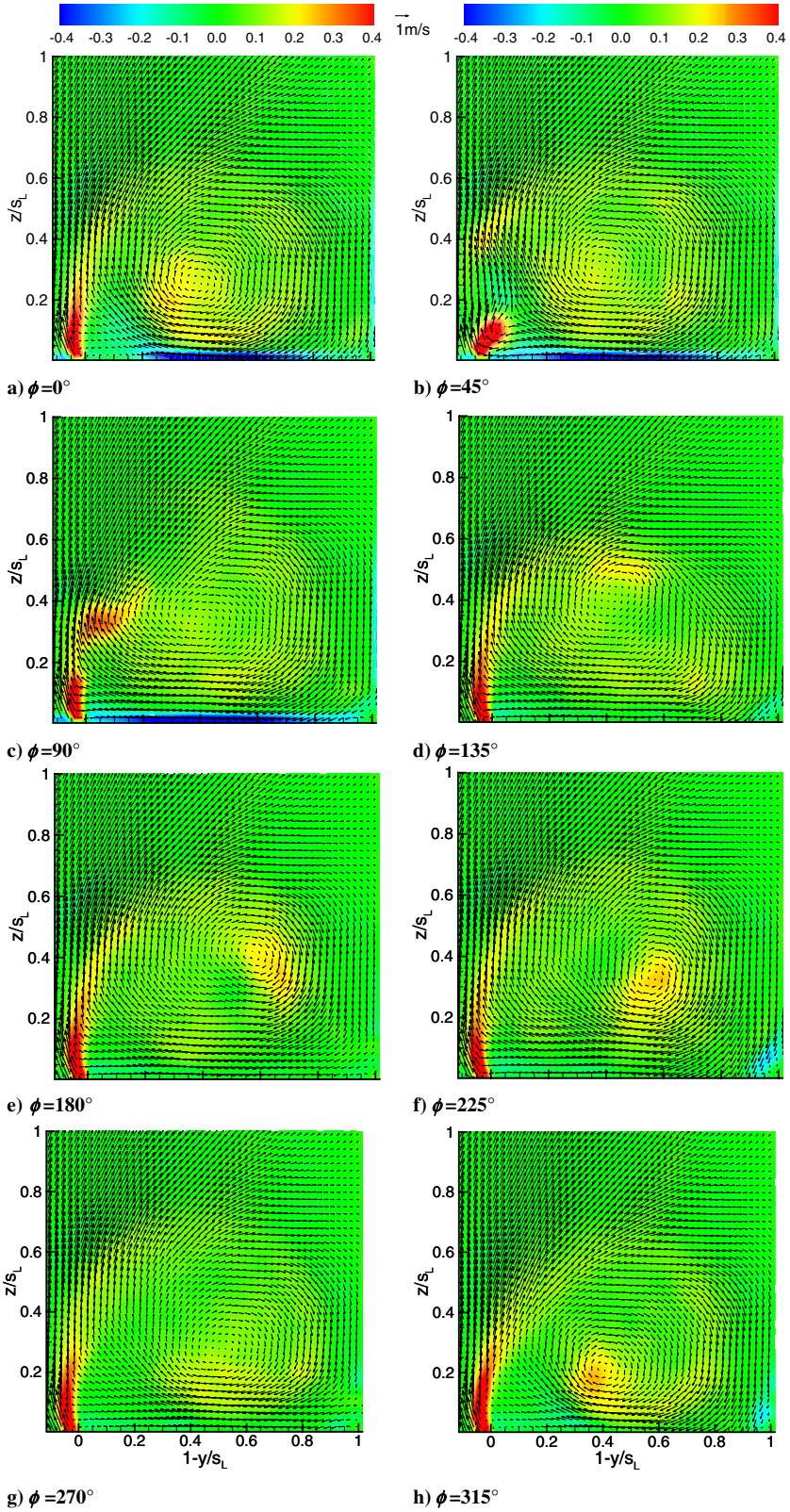

Fig. 8 Phase-averaged PIV vorticity ($\omega_x \times 1000$) and velocity vectors at $\alpha = 36$ deg, $x/c = 0.5$, and $Re = 20,000$; $F^+ = 1$ and DC = 10% in the y–z plane; shown at 45-deg phase differences.

Acknowledgments

The authors wish to thank B. Göksel (Electrofluidsystems, Ltd.) for supplying the high-voltage generators used in this study and for providing support relating to the development of dielectric barrier discharge actuators. The authors also wish to thank D. Romann, A. Lacarelle, S. Vey, and C. Y. Schüle for assistance with the optical measurements presented herein.

References

[1] Mitchell A. M., and Delery J., "Research into Vortex Breakdown Control," *Progress in Aerospace Sciences*, Vol. 37, No. 4, May 2001, pp. 385–418.
doi:10.1016/S0376-0421(01)00010-0

[2] Gursul I., "Review of Unsteady Vortex Flows over Slender Delta Wings," *Journal of Aircraft*, Vol. 42, No. 2, 2005, pp. 299–319.

[3] Mitchell, A. M., Molton, P., Barberis, D., and Delery J., "Vortical Substructures in the Shear Layers Forming Leading Edge Vortices," 19th Applied Aerodynamics Conference, Anaheim, CA, AIAA Paper 2001-31012, June 2001.
[4] Margalit, S., Greenblatt, D., Seifert A., and Wygnanski I., "Delta Wing Stall and Roll Control Using Segmented Piezoelectric Fluidic Actuators," *Journal of Aircraft*, Vol. 42, No. 3, 2005, pp. 698–709.
[5] Guy Y., Morrow J. A., and McLaughlin T. E., "Velocity Measurements on a Delta Wing with Periodic Blowing and Suction," AIAA Paper 2000-0550, 2000.
[6] Siegel S. G., Mclaughlin T. E., and Morrow J. A., "PIV Measurements on a Delta Wing with Periodic Blowing and Suction," AIAA Paper 2001-2436, 2001.
[7] Siegel S. G., Mclaughlin T. E., and Albertson J. A., "Partial Leading Edge Forcing of a Delta Wing at High Angles of Attack," AIAA Paper 2002-3268, 2002.
[8] Corke, T. C., He C., and Patel, M.P., "Plasma Flaps and Slats: An Application of Weakly Ionized Plasma Actuators," 2nd AIAA Flow Control Conference, Portland, OR, AAIA Paper 2004-2127, 2004.
[9] Enloe, C. L., McLaughlin, T. E., Van Dyken, R. D., Kachner, K. D., Jumper, E. J., and Corke, T. C., "Mechanism and Responses of a Single Dielectric Barrier Plasma Actuator: Plasma Morphology," *AIAA Journal*, Vol. 42, No. 3, 2004, pp. 589–594.
[10] Göksel, B., Greenblatt, D., Rechenberg I., Nayeri, C. N., and Paschereit, C. O., "Steady and Unsteady Plasma Wall Jets for Separation and Circulation Control," 3rd AIAA Flow Control Conference, San Francisco, CA, AIAA Paper 2006-3686, June 2006.
[11] Greenblatt, D., Göksel, B. Schüle, C. Y., and Paschereit, C. O., "Dielectric Barrier Discharge Flow Control at Very Low Flight Reynolds Numbers," *47th Israel Annual Conference on Aerospace Sciences* [CD-ROM], Faculty of Aerospace Engineering, Technion–Israel Inst. of Technology, Haifa, Israel, Feb. 2007.
[12] Greenblatt, D., Göksel, B., Rechenberg, I., Schüle, C. Y., Romann, D., and Paschereit, C. O., "Dielectric Barrier Discharge Flow Control at Very Low Flight Reynolds Numbers," *AIAA Journal*, Vol. 46, No. 6, 2008, pp. 1528–1541.
[13] Greenblatt, D., Kastantin, Y., Nayeri, C. N., and Paschereit, C. O., "Delta Wing Flow Control Using Dielectric Barrier Discharge Actuators," 25th AIAA Applied Aerodynamics Conference, Miami, FL, AIAA Paper 2007-4277, June 2007.
[14] Greenblatt, D., and Wygnanski, I., "Control of Separation by Periodic Excitation," *Progress in Aerospace Sciences*, Vol. 36, No. 7, 2000, pp. 487–545.
doi:10.1016/S0376-0421(00)00008-7
[15] Greenblatt, D., and Washburn, A., "Influence of Finite Span and Sweep on Active Flow Control Efficacy," *AIAA Journal* (to be published); also AIAA Paper 2007-4275, June 2007.
[16] Naveh, T., Seifert, A., Tumin, A., and Wygnanski, I., "Sweep Effect on Parameters Governing Control of Separation by Periodic Excitation," *AIAA Journal*, Vol. 35, No. 3, 1998, pp. 510–512.

F. Coton
Associate Editor